IEEE Access
Multidisciplinary | Rapid Review | Open Access Journal

Received March 26, 2022, accepted April 14, 2022, date of publication April 25, 2022, date of current version May 6, 2022.

Digital Object Identifier 10.1109/ACCESS.2022.3170044

A Critical Analysis of Bifacial Solar Farm Configurations: Theory and Experiments

JABIR BIN JAHANGIR[1], (Graduate Student Member, IEEE), MD. AL-MAHMUD[1], MD. SHAHADAT SARKER SHAKIR[1], ANISUL HAQUE[1], (Senior Member, IEEE), MUHAMMAD A. ALAM[2], (Fellow, IEEE), AND M. RYYAN KHAN[1], (Member, IEEE)

[1]Department of Electrical and Electronic Engineering, East West University, Dhaka 1212, Bangladesh
[2]School of Electrical and Computer Engineering, Purdue University, West Lafayette, IN 47907, USA

Corresponding author: M. Ryyan Khan (ryyan@ewubd.edu; ryyan.khan.eee@gmail.com)

This work was supported by the East West University Center for Research and Training (EWU-CRT) under Grant EWUCRT (RP)-11(11)-5/2018.

ABSTRACT The bifacial photovoltaics (PV) technology promises several advantages over monofacials, including improved energy yield, lower operating temperature, and easier integration with agrophotovoltaics. There have been various experimental or computational studies comparing bifacials to monofacials; however, a theory-experiment combined analysis for accurate worldwide extrapolation is missing. Literature review reveals that many reported experiments study standalone systems that overrepresent the yield performance obtainable in farms. Moreover, most reported experimental studies are for configurations that are not necessarily designed close to the optimum. In this work, we experimentally study and analyze the fixed-tilted bifacial farm configiurations, namely south-facing monofacial, south-facing tilted bifacial (TBF), and ground-sculpted vertical bifacial (VBF) arrays, at Dhaka, Bangladesh (23.7 °N, 90.4 °E). The optimal TBF configuration, for 0.5 albedo, yields 21.3% and 73.3% more than the optimal monofacial and the optimal VBF configurations, respectively. Through a combination of experimental and numerical analysis, we compare the in-array performance of the configurations under different albedo conditions to analyze the physics and consolidate the predictions. There is a growing interest in PV array configurations beyond the conventionally ground-mounted south-facing TBF, such as agrophotovoltaics, floating-PV, industry-roof PV array, etc. This necessitates a critical analysis of various array configurations for broader PV expansion.

INDEX TERMS Bifacial, energy yield, experiment, ground-sculpting, photovoltaics, solar farm, simulation, tilted, vertical.

I. INTRODUCTION

According to the 2020 International Technology Roadmap for Photovoltaics (ITRPV), the worldwide market share of bifacial solar cells is expected to grow from 20% in 2020 to 70% by 2030 [1]. This significant increase is attributed to the intrinsic bifaciality of newer commercial solar cell technologies, such as PERC, PERT, and HIT [2]. As these bifacial cells become inexpensive, they will also heighten the interest in bifacial modules. Bifacial modules are projected to be the dominant technology for the proposed next-generation solar farms in the Middle-East and South America [3], [4]. Deployment of bifacial systems is expected to decrease the Levelized cost of energy (LCOE) with its inherently better light collection and increased energy yield [5].

The associate editor coordinating the review of this manuscript and approving it for publication was Lorenzo Ciani.

The design and setup of bifacial farms for optimal LCOE and yield depend on the geographical conditions. While it is imperative to understand the optimal bifacial array designs for traditional, utility-scale, grid-connected solar farms—unconventional array configurations under local irradiance conditions may also play a role in creating a sustainable system. For example, vertical module arrays are only viable with bifacial modules. Although vertical setups have lower output shown experimentally [6] and numerically [7], this configuration may be used to mitigate soiling in highly dust prone regions [8], [9], and in agrophotovoltics (agro-PV) [10], [11]. New farm topologies involving bifacial tracking, floating bifacials, bifacials in agro-PV, etc. may be the next-generation systems enabled through the development of bifacial technology and industry [12]. As a result, several groups have published theoretical and/or experimental results, but these works have typically focused on experimental or theoretical

results related to a single farm topology. An integrated theory-experiment analysis comparing multiple topologies is generally not reported—making it difficult to quantify the relative bifacial gain of the possible farm topologies under comparable operating conditions.

A. STANDALONE PV SYSTEMS

Regardless of the chosen topology, the energy yield performance of bifacial modules compared to the conventional monofacial ones is improved due to additional light collection at the rear face. The fraction of solar irradiance incident on the rear face of a bifacial module mainly depends on the albedo of the ground surface underneath. Thus, the yield of bifacial systems can improve by controlling the ground (i.e., reflector) geometry as well as increasing the reflectance. For example, one of the early studies on standalone bifacial modules by Cuevas *et al.* presented the great promise of bifaciality by demonstrating a 50% bifacial gain when the system was mounted over a white ground with a white wall as a reflector [13]. In South Korea, experiments with standalone systems showed bifacial gain of 5.25%, 11.10%, and 14.47% for albedo $R_A = 0.06$, 0.12, and 0.21 for different surface materials [14] — the gain is observed to reach 33.3% for $R_A = 0.79$ [15]. The numerical analysis by Sun *et al.* [16] found that a 30% bifacial gain for tilted bifacial configurations is obtainable worldwide with 1-meter module elevation for $R_A = 0.5$. Expectedly, this yield-albedo relationship is extensively reported in the literature for different locations and surface materials. However, many experiments up to date are carried out with standalone systems as opposed to modules in-array configurations [17]. A standalone system can receive light unobstructed by any adjacent structure, therefore, constitute an overoptimistic representation of the conditions in a solar farm.

B. ENERGY YIELD FROM ARRAYS ARE LOWER THAN STANDALONE SYSTEMS

For a module in a multi-row array with optimal pitch, the shadings from adjacent modules and rows of modules reduce the rear-irradiance, leading to a lower energy yield than the standalone systems. For south-facing tilted bifacial (TBF) arrays with 4.5-meter row spacing, Baloch *et al.* reported a 5.88% decrease in specific yield compared to a standalone bifacial system [18]. The effect of limited albedo collection from a period was numerically shown by Berrian *et al.* [19]. They estimate that the 24% bifacial gain in energy of a standalone system can reduce to ∼16.5% in an array configuration. Further, simulations with a raytracing model show that at Albuquerque, a single isolated module receives 45% more rear-irradiance compared to when placed in a single row [17]. In a multi-row system, the rear-face irradiation of the center module can be ∼30% lower than that of the modules at the edges. As a result, the results observed in the host of experiments for standalone bifacial systems found in literature cannot be extrapolated to predict bifacial PV farm yield. Moreover, experiments should be studied alongside numerical models to understand the validity and accuracy of extrapolated worldwide predictions.

C. GROUND SHAPING CAN IMPROVE ARRAY OUTPUT

In addition to increasing the bifacial yield by engineering surface material and albedo, we may also improve the bifacial yield by engineering the ground geometry [13], [20], [21]. Such strategies are expected to increase the rear-face irradiance by driving more light towards the modules. As mentioned earlier, Cuevas *et al.* placed a white reflective wall at the back and achieved an extra-ordinary 50% bifacial gain [13]; however, such an arrangement is not suitable for outdoor TBF arrays. A more practical option was proposed by Nussbaumer *et al.* [21], where the ground below the module array would have a periodic-parabolic pattern. A vertical bifacial (VBF) array is expected to have more benefit from engineered ground shape, as the yield of vertical modules is significantly dependent on albedo collection due to its high tilt angle. In the ground-sculpted vertical bifacial (VBF) layout proposed by Khan *et al.* [22], the ground underneath the array is shaped to enhance albedo collection by the vertically mounted modules (see Fig. 1(b)). The authors predicted that, with $R_A = 0.5$, optimal VBF farms can outperform optimal monofacial farms in most locations on the earth having clearness index, $k_t < 0.45$. However, the numerical analysis omits Perez correction [23] in the insolation model and the performance predictions are yet to be experimentally validated.

D. THE NEED FOR OPTIMUM/COMPREHENSIVE EXPERIMENTS

Table 1 shows that the existing literature of bifacial farms involves an eclectic mix of topology, technology, and albedo-related results that makes direct comparison difficult. Moreover, the experimentally tested TBF configurations found in the literature may not necessarily be optimized. Patel *et al.* [24] predicts 15–20% bifacial gain for arrays optimized for tilt (β), period (p), and fixture elevation (y_0) at latitude <30°. A VBF solar farm designed for maximum output *per land area*, however, yields 10–40% less than an optimal monofacial farm close to the equator [25]. With an increased row-spacing, the albedo collection significantly improves, and the VBF becomes competitive to monofacials. It is important to realize that the bifacial gain of *each module* may increase in an array if the row-spacing is increased—this is due to enhanced albedo collection. However, this will in turn reduce the overall yield and bifacial gain of *the finite-area farm* due to the reduced number of modules. The experimental studies should therefore be designed accordingly close to the optimal configuration.

E. THE KEY GAPS IN LITERATURE

The important issues unaddressed in literature can be summarized as follows. (i) There are very few experiments on bifacial PV arrays. (ii) These studies are away from optimum, resulting in an unclear understanding of the expected bifacial gain. (iii) The array experiments at each location focus on

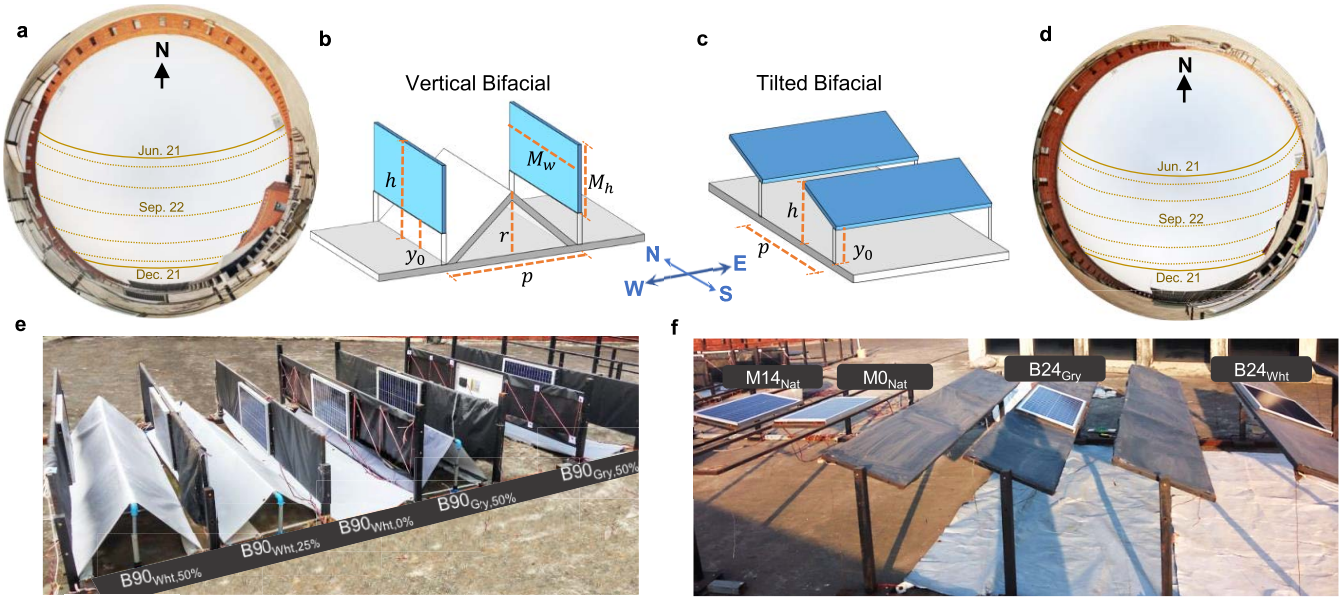

FIGURE 1. **a and d, View of the sky dome and approximate sun-paths as seen from the VBF and TBF array, respectively. b–c, Schematic showing parameters of VBF and TBF array configurations. e, Test array for ground-sculpted vertical bifacial configuration. The image shows the triangular-prism shaped ground covered with vinyl banners with different albedo. From left, the configurations shown are $B90_{Wht,\,50\%}$, $B90_{Wht,\,25\%}$, $B90_{Wht,\,0\%}$, $B90_{Gry,\,50\%}$ and $B90_{Gry,\,0\%}$. f, Test array for south facing tilted bifacial configurations ($B24_{Wht}$, $B24_{Gry}$) and monofacial configurations. The ground underneath is covered with vinyl banners with R_A= 0.3 and 0.5 (from left). The adjacent rows and module slots of bifacial modules are covered with opaque vinyl banners to emulate in-array conditions. In all the experiments, we emulate a bifacial module using two monofacial modules, which allows us to decouple outputs from the two faces [34].**

a single configuration, so that energy yield of multiple configurations cannot be compared. (iv) The experiments and numerical models are not self-consistently tested for model validations. (v) In addition to the disjoint set of experiments in literature, the bifacial gain is sometimes defined as the energy gained from a bifacial module compared to a monofacial one oriented at the same angle [17], [26]. However, it is more useful to compare the energy gain of optimum bifacial topology compared to that of optimum monofacial one [5] — we will use this definition (also shown later in Eq. 1).

In this work, we present a theory-experiment combined study of near-optimum fixed-tilted bifacial array topologies under the same ambient conditions. Ten array configurations (summarized in Table 2) have been set up for this study. This includes seven bifacial and three monofacial configurations. Here, we report the outdoor energy yield performance of the south-facing fixed-tilted bifacial (TBF) and ground-sculpted east-west-facing vertical bifacial (VBF) array configurations using small-scale setups. Our miniaturized test arrays are predictive of its larger counterpart [32], [33]. We measure and analyze both the effects of varying albedo and ground shaping on bifacial gain. The same set of configurations are also modeled using Purdue view-factor (VF)-based optoelectric solar farm model [5], [22]. The experimental results provide the basis for validation of the model for solar farms and the model's subsequent application in the spatio-temporal extrapolation of farm performance across the globe. The paper is organized as follows.

Sec. II: Description of the experimental array configurations under study
Sec. III: Analysis of measured minute-by-minute output variation on clear and cloudy days
Sec. IV: Analysis of measured daily yield and relevant statistics
Sec. V: Overall yield comparison integrated over the analysis period and validation of numerical results
Sec. VI: Location-specific performance of optimum bifacial solar farms
Sec. VII: Discussion on the effect of diffuse sunlight on optimal VBF performance

II. EXPERIMENTAL ARRAY CONFIGURATIONS

The contributions from the front and the rear faces of an in-field bifacial module cannot be decoupled without additional equipment. A workaround to this problem is to use two monofacial modules to represent each face of the bifacial module. Previously, Hansen *et al.* [34] adopted a similar approach to analyze rear-face irradiance. When two identical monofacial modules are used, the resultant emulated bifacial module will have a unity bifaciality factor. For this experiment, we chose Solarland's SLP030-12 monofacial modules with 30 W nominal maximum power. Each module has a length (M_w) of 26.57 inches and width (M_h) of 14 inches.

We consider parametric variations of east-west facing, ground-sculpted vertical bifacial (VBF) module array and south-facing bi-/mono-facial module array for this experiment, see Fig. 1. Our setup consists of two miniaturized

TABLE 1. Bifacial gains of fixed-tilted systems reported in literature for varying design parameters.

Location	Type	Orientation	Tilt β (°)	Minimum elevation, y_0 (m)	Ground albedo, R_A	Bifacial gain in energy [a] (%)	Remarks
El Gouna, Egypt [27]	Standalone	South	20	1.2	0.3	20.53	5-month average bifacial gain
Albuquerque, USA [26]	Standalone	South	15 25 35 45	N/A	0.2-0.3	11.8 12.3 15.4 19	Bifacial gain considering a month of data
Albuquerque, USA [26]	Standalone	East/West	90	N/A	0.2-0.3	∼-7.69 (116)[b]	One year of data; gain relative to best monofacial
South Korea [15]	Standalone	South	30	1	0.21 0.79	10.5 33.3	N/A
South Korea [14]	Standalone	South	30	N/A	0.06 0.12 0.21	5.25 11.10 14.47	N/A
Linköping, Sweden [6]	Standalone	South	40	N/A	0.05	5	N/A
Linköping, Sweden [6]	Standalone	East/West	90	N/A	0.05	1	N/A
Thuwal, Saudi Arabia [28]	Standalone	South	25 45	0.2	Gray gravel (0.2–0.3)[c]	10 15	N/A
Doha, Qatar [18]	Standalone	South	22	1	0.2 0.4 0.6	∼18 ∼20 ∼27	90% module bifaciality factor (BF)
Doha, Qatar [18]	Standalone	South	90	1	0.2 0.4 0.6	∼8 ∼18 ∼28	90% module BF
Doha, Qatar [18]	Standalone	East/West	90	1	0.4	∼2	90% module BF
Doha, Qatar [18]	Array	South	22	1	0.4	8.6 (60% BF) 16.3 (90% BF)	5.88% relative yield loss in array compared to standalone configuration
Golden, USA [29]	Array (3 rows)	South	10	0.15 0.4	0.56-0.7	5-10 5-25	N/A
Hokkaido, Japan [30]	Array (3 rows)	South	35	1.5	Grass (0.25)[c] Snow (0.7-0.9)[c] Scallop's shell (∼0.7-0.9)[c] Scallop's shell and snow (∼0.7-0.9)[c]	8.6 23 23.3 23.9	N/A
Austria [31]	Array (4 rows)	East/West	N/A	0.4	White paint (0.5-0.9)[c]	15-20	70% module BF
Dhaka, Bangladesh *(this work)*[d]	Array	South	24	0.56	0.3 0.5	18.3 21.3	∼2-month experiment, annual numerical prediction.
Dhaka, Bangladesh *(this work)*[d]	Array	East/West	90	0.15	0.3 0.5	-39.8 -30.0	∼2-month experiment, annual numerical prediction.

a. Bifacial gain in energy relative to south-facing tilted monofacial configuration. A slight exception are the gains reported in this work for Dhaka (last row) where it is defined relative to the yield of *optimum* monofacial configuration (see Eq. 1)
b. Bifacial gain in energy relative to identically oriented monofacial configuration as reported in the literature
c. Typical albdeo values for the surface material
d. Bifaciality is emulated using two monofacial modules for provision of separate analysis of light collection by the two faces.

test arrays on the rooftop of East West University (23.7° N, 90.4° E) in Dhaka, Bangladesh. The first array shown in Fig. 1(e), oriented east-west ($\gamma = 90°$), hosts vertical bifacial modules with the triangularly shaped ground. The second array shown in Fig. 1(f), oriented south ($\gamma = 0°$), hosts tilted bifacial and the monofacial modules. We study ten array configurations in this work, listed in Table 2. The relevant design parameters are defined in Fig. 1(b, c).

The naming convention for the configurations is as follows. The first letter indicates a bifacial (B) or monofacial (M) module setup. Then, the module β follows: a value of 90 indicates an east-west oriented VBF, and a value less than 90 indicates a south-oriented tilted bi-/mono-facial array. The subscripts indicate the ground albedo and, additionally for VBFs, the ground height ratio H_R.

The vertical bifacial test array has five east-west-facing VBF configurations: $\mathrm{B90}_{Gry,\ 0\%}$, $\mathrm{B90}_{Gry,\ 25\%}$, $\mathrm{B90}_{Wht,\ 0\%}$, $\mathrm{B90}_{Wht,\ 25\%}$, and $\mathrm{B90}_{Wht,\ 50\%}$. Here, the subscripts 'Wht' and 'Gry' indicate the color of the ground underneath each configuration. As shown in Fig. 1(e), a triangular-prism-shaped ground was employed with ground height r between two rows. The numbers in the configuration names indicate the height of the triangularly shaped ground relative to the array height (H_R) (see Table 2). We installed the modules in landscape orientation. The modules were elevated (y_0) at 6 inches above the ground and placed periodically (p) 22 inches apart. Keeping other variables constant, we varied H_R or R_A for each vertical configuration.

The ground albedo was controlled by covering the ground with colored vinyl banners having 50% (white-colored) and 30% (gray-colored) measured reflectance R_A (see Experimental procedures in appendix). To exclude the effect of edge brightening that may result in overestimated yield [26], [27], we mounted the modules on the central slot of the rack in landscape orientation and covered the adjacent ones with black, opaque vinyl banners (see Fig. 1(e,f)). The black

TABLE 2. List of configurations and the corresponding design parameters chosen for the experiment at Dhaka (23.7°N, 90.4°E).

Label	Type	Array Azimuth, γ^a (deg)	Module tilt, β^b (deg)	Ground height, r (in)	Array height, h (in)	Minimum elevation, y_0 (in)	Ground height ratio, $H_R{}^c$ (%)	Array pitch, p (in)	Ground/R_A	Bifacial gain in energy, $BG_E{}^d$ (%)
$M0_{Nat}$	Monofacial	180	0	-	25	25	-	24	Natural	-
$M14_{Nat}$	Monofacial	180	14	-	26.7	23.3	-	24	Natural	Reference
$M24_{Nat}$	Monofacial	180	24	-	28	22	-	24	Natural	-
$B24_{Gry}$	TBF	180	24	-	28	22	-	24	Gray/0.3	18.3
$B24_{Wht}$	TBF	180	24	-	28	22	-	24	White/0.5	21.3
$B90_{Gry,\ 0\%}$	VBF	90	90	0	22	6	0	22	Gray/0.3	−38.9
$B90_{Gry,\ 50\%}$	VBF	90	90	14	22	6	50	22	Gray/0.3	−39.8
$B90_{Wht,\ 0\%}$	VBF	90	90	0	22	6	0	22	White/0.5	−33.7
$B90_{Wht,\ 25\%}$	VBF	90	90	10	22	6	25	22	White/0.5	−32.9
$B90_{Wht,\ 50\%}$	VBF	90	90	14	22	6	50	22	White/0.5	−30.0

a. Azimuth defined with respect to the north
b. Tilt angle from the horizontal plane
c. VBF ground height ratio, $H_R = (r - y_0)/(h - y_0)$ for $r > y_0$
d. Bifacial gain in energy (BG_E) compared to $M14_{Nat}$ configuration after 52-day experimental period

covers artificially create row-to-row shading conditions on a module placed within a large array. In addition to the in-array losses, each configuration will incur a varying degree of output loss due to soiling. To stem such unwanted variability, the modules were manually cleaned every 24 hours.

The south-facing test array hosts two TBF configurations: $B24_{Gry}$ and $B24_{Wht}$. These modules were tilted at 24° with an array period (p) of 24 inches, and minimum ground clearance (y_0) of 22 inches. The albedos (R_A) of the ground underneath the $B24_{Wht}$ and $B24_{Gry}$ configurations are 50% and 30%, respectively.

To compare the outputs of bifacial configurations with conventional south-facing tilted monofacial ones, we have set up two monofacial modules tilted at 0° and 14° angles, which are labeled $M0_{Nat}$ and $M14_{Nat}$, respectively. As the module bifaciality was emulated by back-to-back mounted monofacial modules, we may readily measure the power generated from the front face of a TBF configuration alone. The $M24_{Nat}$ configuration represents the measurement from the front face of a bifacial configuration tilted at 24°.

III. MINUTE-BY-MINUTE ANALYSIS OF DIURNAL OUTPUTS

In this section, we will discuss the characteristics of the minute-by-minute output and the albedo collection at different parts of the day under clear or cloudy weather conditions.

A. TEMPORAL VARIATION IN OUTPUT

We measured each module's short circuit current (I_{SC}) at two-minute intervals from September 24 to November 26, 2019, during late autumn. As shown in Fig. 1(a,d), during the experimental period the sun follows a low-altitude path. For a bifacial configuration, we calculate the total bifacial output by summing the outputs of the front and rear modules. Fig. 2 shows the diurnal I_{SC} profiles (30-sample moving averaged) on three representative days to demonstrate the effects of varying cloud conditions. We quantify the cloud conditions with the corresponding estimated daily diffuse fractions (k_d)

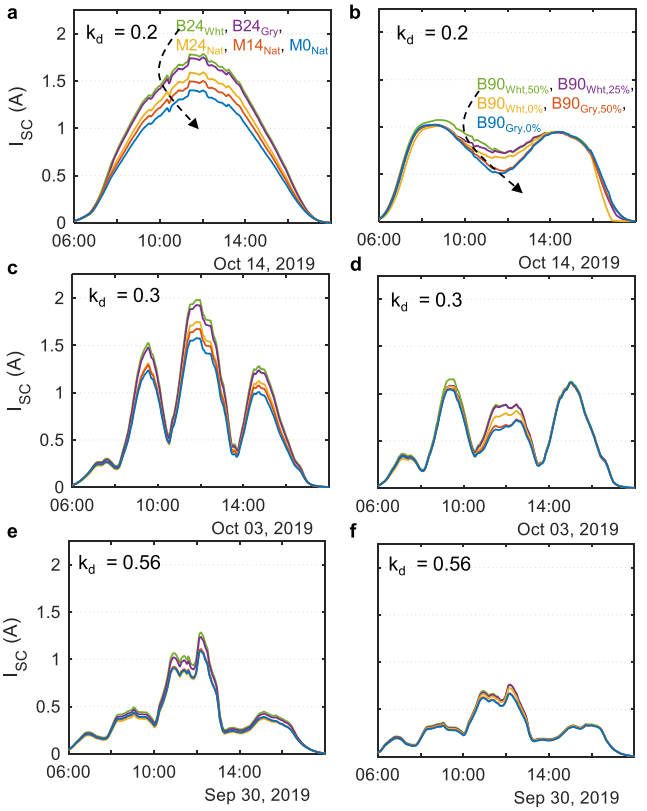

FIGURE 2. The recorded short circuit current, I_{SC}, values from TBF (left column) and VBF (right column) configurations on clear (a and b), partly cloudy (c and d) and rainy day (e-f). The daily diffuse fractions are shown on the plots.

(see Experimental procedures for details) defined as the ratio of daily diffuse and global irradiance on a horizontal plane. A higher k_d indicates a relatively cloudier day.

On a clear day ($k_d = 0.20$), south-facing tilted bifacial (TBF) and monofacial modules show a bell-shaped I_{SC} characteristic with a peak at noon, see Fig. 2(a). On the same day, as shown in Fig. 2(b), the east-west facing vertical

bifacial (VBF) modules show the well-known double-hump profile. At noon, the direct sunlight does not reach any of the module faces, and the output is entirely comprised of albedo and sky-diffuse light – the inability to receive direct light causes the output to dip. A couple of hours before and after noon, one of the module faces can collect the direct sunlight resulting in the double-peaks. All vertical configurations will receive identical direct and diffuse light from the sky; the only difference is in the albedo collection which is controlled by the combined effect of the reflectivity R_A and the ground shape. The difference in output current is therefore prominent in the absence of direct light collection closer to noon. Fig 2(c,d) shows that, on a partly cloudy day ($k_d = 0.30$), the current profiles show frequent fluctuations due to moving clouds. Finally, as shown in Fig. 2(e,f), on an overcast day ($k_d = 0.56$) dominated by diffused sunlight, the diurnal profiles of the vertical and tilted configurations become indistinguishable. The double humps in the vertical modules are no longer visible as there is very little direct sunlight.

B. DECOMPOSED OUTPUT OF MODULE FACES AND THE EFFECT OF ALBEDO

As we have used back-to-back monofacial modules to emulate a bifacial module, we can separately measure and analyze the light collection on each face. Fig. 3 (a,b) show the measured current output of the two faces in TBF ($B24_{Wht}$) and VBF ($B90_{Wht,\ 50\%}$) configurations obtained on October 14, 2019 (clear day). The front face of the TBF configuration faces the sun and collects both the direct and diffuse sunlight, whereas the rear face of TBF collects the albedo and a small fraction of sky-diffuse light. Fig. 3(a) shows the outputs from the individual faces. In Fig. 3(b), the east and west faces of a vertical bifacial (i.e., VBF) show output characteristics mirrored around the solar noon. For example, the west-oriented face (red-line) will not directly see the sun (i.e., no direct sunlight collection) till noon. Therefore, the output current from this face represents only the combined albedo and sky-diffuse light collection before noon. After the solar noon, the west face will collect direct, diffuse, and albedo — that is why there is a significant increase in output beyond noon. We can similarly explain the output from the east face where the direct sunlight is received only before noon. If we want to decouple and remove the direct light collection on the vertical bifacial module, we would only consider the output from the west face before noon, and from the east face after noon, see Fig. 3(d). This gives us the combined collection from sky diffuse and albedo light.

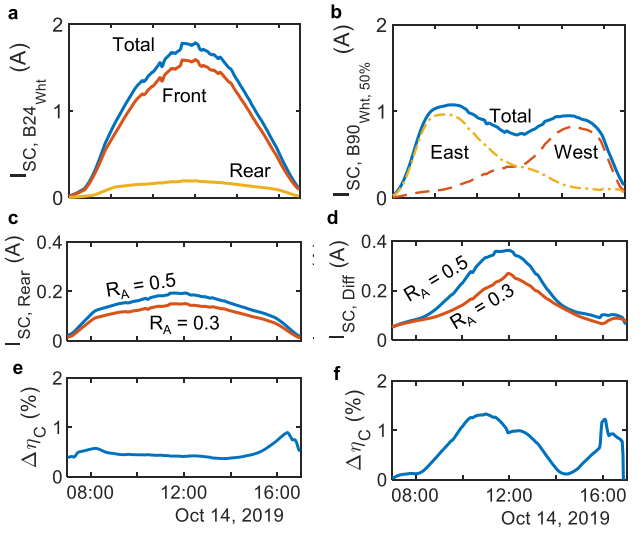

FIGURE 3. Measurements from front and rear faces of TBF (left column) and VBF (right column) configurations on October 14, 2019. a, Measured total I_{SC} and the contributions from front and rear faces of $B24_{Wht}$ configuration. b, Measured total I_{SC} and contributions from the east and west faces of $B90_{Wht,\ 50\%}$. c, Comparison of the TBF's rear face I_{SC} for $R_A = 0.5$ and 0.3. d, Comparison of the diffuse light collection of $B90_{Wht,\ 50\%}$ and $B90_{Gry,\ 50\%}$. e-f, Increase in absolute collection efficiencies ($\Delta\eta_C$) of TBF and VBF arrays due to 20% increase in R_A.

Fig. 3(c, d) show the sky diffuse and albedo contribution to the current for TBF and VBF, respectively. These figures show scenarios for both $R_A = 0.3$ and 0.5. The increase in output current for the $B24_{Gry}$–$B24_{Wht}$ pair (TBF) or the $B90_{Gry,\ 50\%}$–$B90_{Wht,\ 50\%}$ pair (VBF) is only due to the increase in albedo collection originating from increased reflectance from the ground. Over the period on October 14, we observe 10.43% and 2.83% relative increases in energy yield for the VBF and TBF pairs, respectively. The corresponding increase in output power, normalized to GHI, gives the increase in efficiency $\Delta\eta_C$ due to the increased ground albedo R_A (0.3 to 0.5) of the module configurations, see Fig. 3(e, f). Trivially, the $\Delta R_A = 0.2$ increase would translate to an equivalent 20% increase in output. However, this expected gain is significantly suppressed due to module tilt and shading in the periodic array. In practice, we observe $\Delta\eta_C \sim 0.5\%$ for TBF, and $\Delta\eta_C \sim 0.5\%$ to 1.3% (between 9 a.m.–3 p.m.) for VBF. We can read $\Delta\eta_C$ as the absolute increase in efficiency of the relevant module configuration for the tested $\Delta R_A = 20\%$ scenario.

IV. DAILY INTEGRATED YIELD AND GAIN

In this section, we will discuss the output integrated over each day and the corresponding bifacial gain statistics. We will also explain the daily efficiency of the different configurations.

A. DAILY VARIATION IN YIELD

To calculate the energy yield, we mapped the measured I_{SC} to corresponding maximum DC power outputs, P_{max} (see Experimental procedures). The resulting daily output power profiles were then integrated over 9 a.m. to 3 p.m. to obtain the daily DC energy yield produced by each configuration. This period was chosen to avoid row-to-row shading in all setups. Further, Fig. 4(a) shows the daily energy yield (Y) of the best performing VBF, TBF, and the monofacial configurations (i.e., $B90_{Wht,\ 50\%}$, $B24_{Wht}$, $M24_{Nat}$). Significant dips in the trend, e.g., on November 10, are associated with rainy or overcast weather conditions. We find that the TBF($B24_{Wht}$)

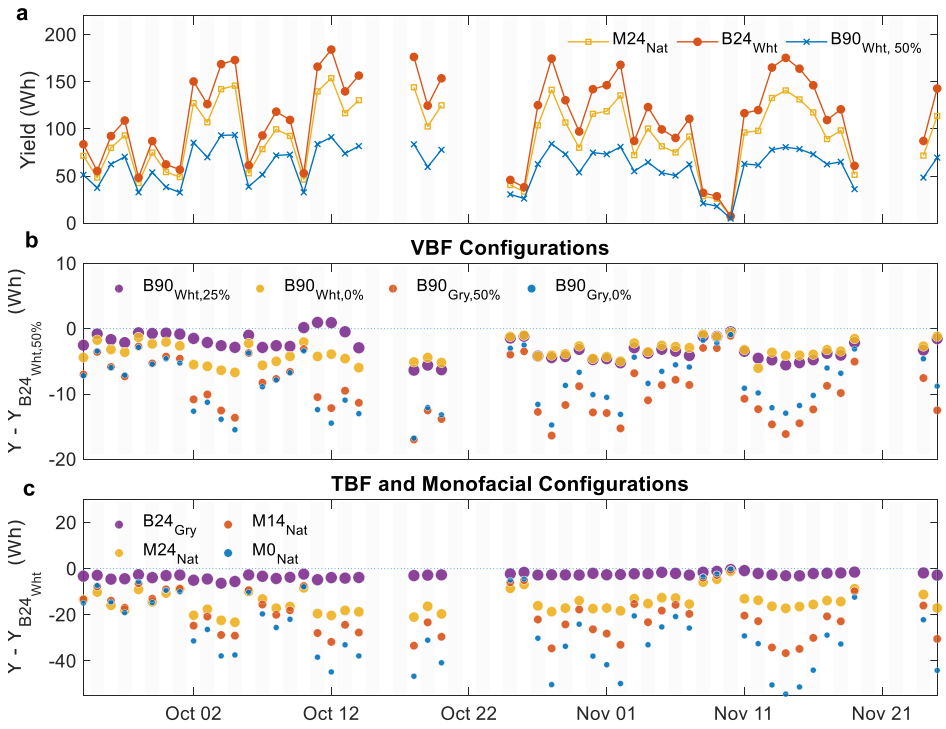

FIGURE 4. Daily energy yields during the 52-day experimental period. a, Daily energy yield of best performing VBF($B90_{Wht,\ 50\%}$), TBF($B24_{Wht}$), monofacial ($M24_{Nat}$) configurations during the period of the experiment. b, Relative daily yield of VBF configurations are shown as the deviations from $B90_{Wht,\ 50\%}$ yield. c, The yield deviations for TBFs and monofacial configurations from $B24_{Wht}$ configurations.

configuration produces the most yield on every day of the experiment, whereas the VBF($B90_{Wht,\ 50\%}$) the least.

The bifacial yield is expected to increase with increasing R_A. Thus, for TBFs, we expect $Y_{B24_{Wht}} > Y_{B24_{Gry}}$ for increasing R_A. For ground-sculpted configurations, as the grounds between the modules are shaped to deflect sunlight towards the adjacent modules (see Fig. 1(e)), we intuitively anticipate that the module's light collection will increase with an increase in r (ground triangle height) provided that the triangular ground shape does not shade the modules. This constraint is satisfied for $H_R \leq 50\%$ [22]. Thus, all else being equal, we expect a higher yield for higher R_A and r. Therefore, among the VBFs, the expected yield performance hierarchy is $Y_{B90_{Wht,\ 50\%}} > Y_{B90_{Wht,\ 25\%}} > Y_{B90_{Wht,\ 0\%}} > Y_{B90_{Gry,\ 50\%}} > Y_{B90_{Gry,\ 0\%}}$. To compare the everyday performance of individual configurations, we plot the daily signed deviations from optimal VBF ($B90_{Wht,\ 50\%}$) and TBF ($B24_{Wht}$) configurations in Fig. 4(b) and Fig. 4(c), respectively. In the figures, we illustrate the expectations by the size of the data markers for each configuration; namely, a larger marker suggests a higher expected yield.

Let us first consider the yield performance of VBF configurations as shown in Fig. 4(b). Negative deviations on most days indicate that the $B90_{Wht,\ 50\%}$ generally performed best as expected. Unexpectedly, on some clear days, e.g., Nov. 12-14, the $B90_{Wht,\ 0\%}$ configuration produced more energy than the $B90_{Wht,\ 25\%}$ (both have the same $R_A = 0.5$). On these days, we observe a more pronounced anomaly for $B90_{Gry,\ 0\%}$ and $B90_{Gry,\ 50\%}$ pair ($R_A = 0.3$) – the output from a flat ground array ($B90_{Gry,\ 0\%}$) crosses over a ground-sculpted one ($B90_{Gry,\ 50\%}$). Such crossovers in yields suggest that a ground-sculpted configuration does not necessarily produce more yield than a non-ground-sculpted one, but depends on the daily weather conditions. We find that the crossovers are correlated with lower values of k_d, i.e., higher availability of direct sunlight. It implies, if a location were to largely receive direct sunlight, the yield enhancement resulting from a sculpted ground may be rendered insignificant. We further examine this implication in a later section.

As for south-facing modules, we expect the bifacial configurations to produce more energy relative to the monofacial ones—since the rear faces of bifacial modules can collect additional light reflected from the albedo enhanced ground. Fig. 4(c) shows daily yield performance trends consistent with our expectation. The south-facing TBF with a white ground ($B24_{Wht}$) demonstrates the highest daily energy yield among the bifacial configurations and consistently outperforms the monofacial ones.

B. BIFACIAL GAIN IN ENERGY

We define the bifacial gain in energy (BG_E) as the fractional gain in the yield of a bifacial array compared to the

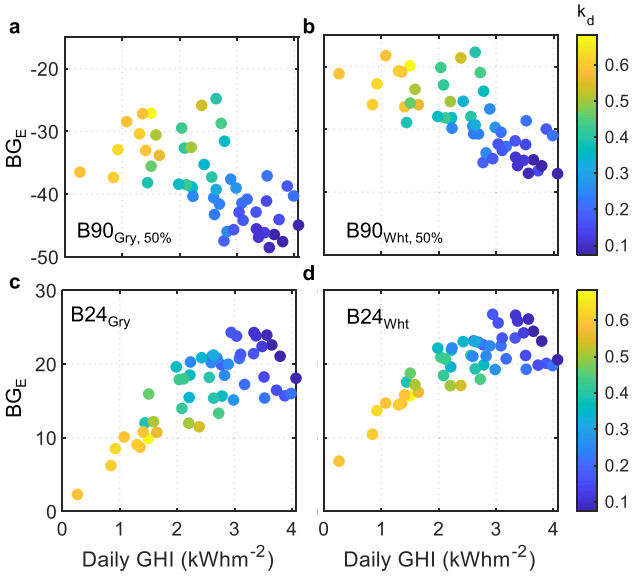

FIGURE 5. Bifacial gain in energy (BG_E) vs. Daily integrated GHI for different configurations. Both daily yield and daily GHI are obtained by integrating the measurements over 9 a.m.–3 p.m. period. Marker colors indicate estimated daily diffuse fractions (k_d).

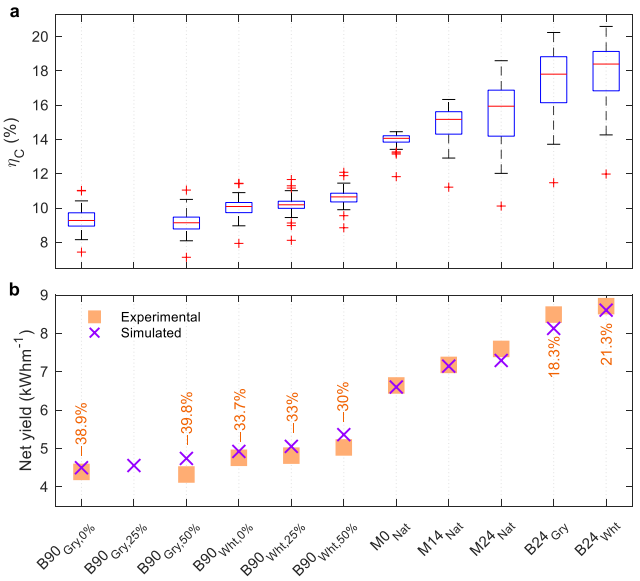

FIGURE 6. a, Boxplots of daily configuration efficiency (η_C) of each setup based on experimental data. b, Experimental and simulated net energy yields per module width of each configuration under study. For each bifacial configuration, the BG_E is shown. For simulations, the OHP model was applied to decompose the measured GHI.

optimum [5] monofacial array:

$$BG_E = \frac{Y_{BF} - Y_{Mono_{opt}}}{Y_{Mono_{opt}}} \times 100 \tag{1}$$

For our location, the optimal monofacial configuration Mono_{opt} is M14_{Nat}. The BG_E-statistics under varying insolation (shown in Fig. 5) can be understood by studying the daily yields and ambient temperatures. As shown in Supplementary Fig. S2, $Y_{\text{M14}_{Nat}}$ linearly increases with GHI. For vertical bifacials, Y_{VBF} vs. GHI slope decreases at higher GHI (see Supplementary Fig. S2), indicating VBF is less efficient under higher GHI. We can also see this in Fig. 5(a, b) where the BG_E for VBF decreases at higher GHI. It is consistent with our previous discussion that VBF performance is better at a higher diffuse fraction (i.e., at lower GHI). As for the bifacial gain in energy for TBFs, we see in Fig. 5(c, d) that the gain is always nonnegative as expected. Interestingly, the BG_E increases with GHI, indicating that TBF is even more efficient under brighter sunlight (clear days). However, the gains have more variability at higher GHI: ∼10% on bright, clear days. This variance can be directly correlated to the broader variance in ambient temperature (hence the module efficiency) as GHI increases, as shown in Supplementary Fig. S4. The daily average ambient temperatures (between 9 a.m.–3 p.m.) at various GHI are shown in Supplementary Fig. S3.

C. DAILY CONFIGURATION-EFFICIENCY

Fig. 6(a) shows the distribution in daily efficiency (module yield per unit area normalized to GHI) for every configuration under study. As M0_{Nat} is placed horizontally, its I_{SC} is proportional to the GHI. The I_{SC}/GHI ratio, therefore, would be constant for any GHI over M0_{Nat}. The spread in M0_{Nat} efficiency is only due to the nonlinear relationship between GHI and P_{max} (i.e., between I_{SC} and P_{max} as shown in Supplementary Fig. S1).

Among the VBFs, the mean efficiency increase with increasing R_A from 0.3 to 0.5 is: (i) 1% between $\text{B90}_{Gry,\ 0\%}$ and $\text{B90}_{Wht,\ 0\%}$, and (ii) 1.5% between $\text{B90}_{Gry,\ 50\%}$ and $\text{B90}_{Wht,\ 50\%}$. On the other hand, the usefulness of ground shaping is not apparent. The efficiency of $\text{B90}_{Gry,\ 50\%}$ (ground sculpted) is marginally lower than $\text{B90}_{Gry,\ 0\%}$ (flat ground), while $\text{B90}_{Wht,\ 50\%}$ performs only marginally better than $\text{B90}_{Wht,\ 0\%}$.

The TBF configurations are 6-7.5% (absolute) more efficient compared to VBFs. The TBFs have larger variability in efficiency than vertical arrays. This again can be associated with the GHI–P_{max} nonlinear relationship. As M24_{Nat}, B24_{Gry} and B24_{Wht} are optimally tilted to collect direct light (compared to M0_{Nat} or M14_{Nat}) during the experimental period (September-November) at the test site, they will cycle through a larger range in I_{SC} when the daily GHI changes. This translates to a larger variation in operating efficiency, see Supplementary Fig. S4. On the other hand, VBFs are less sensitive to direct sunlight. Therefore, the vertical arrays will have a smaller variation in efficiency, mostly associated with ambient temperature variations (shown in Supplementary Fig. S4).

Overall, from the daily yields, we expectedly see that B24_{Wht} has the highest output, and the improvement from ground sculpting in VBF is weather-dependent. The bifacial gain BG_E increases for TBF and decreases for VBF with increasing GHI. And, TBFs have over 5% (absolute)

variabilities in configuration efficiency due to the nonlinear relationship between P_{max} and GHI.

V. NET ENERGY YIELDS OF THE CONFIGURATIONS

In this section, we will compare the net yield of the comparison over the entire study period. Corresponding numerical results present the accuracy of the prediction models. Then the numerical models are used to extrapolate to the annual yields of every configuration.

A. NET ENERGY YIELD OVER THE STUDY PERIOD

The net yield, calculated by summing the daily outputs, will give a better statistical comparison among the various array configurations. Fig. 6(b) shows the net yield per row length ($kW{\cdot}h{\cdot}m^{-1}$) from each configuration for the entire duration of the experiment. Both the experimentally measured (■-marker) and numerically simulated (×-marker) energy yields are shown in the figure.

First, from the experimental data, the trend shows that south-facing tilted bifacial modules ($B24_{Gry}$ and $B24_{Wht}$) produce a higher yield than the monofacial modules, which is expected from our previous discussion. The $B24_{Wht}$ configuration with the white ground ($R_A = 0.5$) shows 21.3% BG_E compared to the $M14_{Nat}$ monofacial configuration; followed by the $B24_{Gry}$ configuration which shows an 18.3% gain. By contrast, among the vertical setups, the best performing VBF configuration $B90_{Wht,\ 50\%}$ ($R_A = 0.5$, $H_R = 50\%$) [22] generates 30% *less* yield than $M14_{Nat}$. It follows that all the TBF configurations produce more energy than the VBF configurations: for the same albedo $R_A = 0.5$, the $B24_{Wht}$ configuration produces 73.3% more yield than $B90_{Wht,\ 50\%}$.

Second, it is apparent that the yield from a bifacial module increases for higher albedo: compare $B90_{Gry,\ 0\%}$ vs. $B90_{Wht,\ 0\%}$, $B90_{Gry,\ 50\%}$ vs. $B90_{Wht,\ 50\%}$, and $B24_{Gry}$ vs. $B24_{Wht}$ in Fig. 6(b). For example, $B24_{Wht}$ with the white-colored ground ($R_A = 0.5$) yields 2.6% more than $B24_{Gry}$ with the gray-colored ground ($R_A = 0.3$). Likewise, the $B90_{Wht,\ 50\%}$ configuration produces 16.3% more than the $B90_{Gry,\ 50\%}$ configuration. Hence, the artificial albedo enhancement effectively increases the yield of bifacial configurations.

Finally, the trends among the vertical modules illustrate the benefits of employing the ground-sculpting technique and the impact of the choice of ground height (r) on VBF performance. The ground-sculpted $B90_{Wht,\ 50\%}$ configuration with 50% H_R shows 5.7% performance improvement over the flat-grounded $B90_{Wht,\ 0\%}$ configuration ($H_R = 0$). Despite the several crossovers observed in the daily yields, i.e., $Y_{B90_{Wht,\ 0\%}} > Y_{B90_{Wht,\ 25\%}}$ on some days, $B90_{Wht,\ 25\%}$, on the whole, produces more yield than $B90_{Wht,\ 0\%}$. However, $B90_{Gry,\ 50\%}$ surprisingly produces slightly less (1.6%) than $B90_{Gry,\ 0\%}$. This anomaly may be due to measurement inaccuracies or by one of the $B90_{Gry,\ 0\%}$ modules receiving marginally higher spurious light from the surroundings. This is plausible because the sun follows a low altitude path during the experimental period (see Fig.1(a,d)) and the presence of building structure in the proximity of the test-site.

B. NUMERICAL PREDICTION OVER THE STUDY PERIOD

Developing simulation tools for bifacial farms is uniquely challenging due to the need to quantify the rear face irradiance. Several bifacial models have been proposed that utilize ray-tracing [29] or the view-factor method [16], [25], [35]–[38]. When compared with field data, both the ray-tracing method and view-factor-based models were found to be in good agreement [39], [40].

We have carried out simulations of the experimental configurations for comparison and yearly predictions. We use the detailed physics-based Purdue view-factor-based solar farm model [5], [22] (summarized in Experimental procedures) to find the numerical results. For the simulations, physical module dimensions and array geometry were chosen and module efficiencies for direct (η_{dir}) and diffuse (η_{diff}) light collection were set to 12.5%. For irradiance inputs, we decompose the on-site measured global horizontal irradiance (GHI) (detailed in Experimental procedures) into direct normal irradiance (DNI) and diffuse horizontal irradiance (DHI) components. The decomposition was performed using a combination of Orgill-Hollands [41] and Perez's [23] anisotropic diffuse skylight model, which we will refer to as the OHP model. We choose the Perez model due to its relatively accurate diffuse sunlight estimation [16], [42]–[44]. The simulations were carried out over the same dates as the experiments for proper comparison.

In addition to the experimental configurations, we also simulate the $B90_{Gry,\ 25\%}$ configuration having identical design parameters to $B90_{Wht,\ 25\%}$, but R_A set to 0.3. As shown in Fig. 6(b), the predicted trend demonstrates an overall good fit to experimental data with 3.8% mean absolute percentage error (MAPE). For TBF and monofacial configurations, the MAPE is 2.7% and 1.7%, respectively. We notice a larger deviation (5.5% MAPE) for the ground sculpted VBFs compared to other configurations. As the yield of vertical bifacials is predominantly controlled by the effective collection of diffuse and albedo light, the accuracy of numerical models for VBF is greatly affected by the accuracy of DHI estimation.

C. PREDICTING ANNUAL YIELDS

We now apply our solar farm model to predict the annual yield of the configurations at Dhaka. For the annual yield simulation (and simulations hereafter), the input daily irradiance data was obtained from NASA's POWER database [45]. As the dataset only provides the daily average GHI, the diurnal GHI profiles are numerically estimated by Haurwitz clear sky model [46] scaled to match the daily average. The aforementioned OHP model was used to decompose the GHI values and estimate the diffuse irradiance component.

The predicted annual yields per row length ($kW{\cdot}h{\cdot}m^{-1}$) for the configurations are shown in Fig. 7(a). We find that the overall yield performance hierarchy of the configurations remains unchanged from the experiments done in Autumn

(shown in Fig. 6): we predict larger yields from the TBF configurations compared to the VBF ones. The seasonally varying availability of diffuse sunlight has an appreciable effect on the performance of the bifacial modules. For instance, during the wet season, a larger fraction of the sunlight will be diffused owing to cloudy sky conditions. To examine the impact of seasonal k_d variations on the yields, we split the annual yield into two six-month periods, named Summer (Apr.-Sept.) and Winter (Oct.-Mar.). The two periods experience approximately equal insolation: the integrated GHI is only ∼3% higher in Summer compared to Winter. However, the periods have a varying degree of availability of diffuse sunlight: the mean daily k_d during the Summer period is 0.53, while it is 0.33 during the Winter.

The trends for Summer and Winter periods in Fig. 7(a) show that, although the ground-sculpted configurations (e.g., $B90_{Wht,\ 50\%}$, $B90_{Gry,\ 50\%}$) perform similarly during both periods, the flat-ground configurations (i.e., $B90_{Wht,\ 0\%}$, $B90_{Gry,\ 0\%}$) perform marginally better (∼7% higher) during Winter when k_d is lower. This predicted yield improvement suggests that direct sunlight conditions are favorable to the vertical bifacial configuration with no ground-sculpting. We will later show that such dependency will have a decisive impact on ground-sculpted vertical farm design based on geographic location. Furthermore, the seasonal yield predictions in Fig. 7(a) indicate that the TBF configurations perform worse during the Summer: $B24_{Wht}$'s yield falls 17% compared to the Winter period. Such decline occurs due to the combined effect of the reduced availability of direct sunlight and slight misalignment between the module and the sun-path during Summer. As such, the relative gain of TBF compared to VBF also declines during this period.

Fig. 7(b) shows the predicted annual yield *per land area* (in kW·h·m^{-2}) of our experimental setup. We obtain the yield per land area for each configuration by dividing their yields in Fig. 7(a) by the respective array pitch (p) parameters. While the TBF gains remain unchanged from Fig. 7(a), they increase for the VBFs. This is because, while TBFs and monofacial arrays have equal array pitch ($p = 24$ in), a slightly smaller period ($p = 22$ in) was chosen for VBFs (see Table 1). Still, the VBFs are predicted to produce less yield per land area than the monofacial configurations at this location. The relative improvement in yield per land area of the densely packed VBF will be considered at higher latitudes when the monofacial modules are optimally tilted higher with increased row-spacing. That is why VBFs are preferred at higher latitude [25] as it maximizes *output per land area* in a finite-sized farm.

The net yield of the configurations discussed in this section provides some key insights: an increase in R_A from 0.3 to 0.5 increases BG_E of TBF by 3% (18.3% to 21.3%). The numerical results for TBF and VBF are within 2.7% and 5.5% of the experiments. Our numerical predictions over different seasons show that: (i) TBF in this location performs better under lowered diffuse light, and (ii) ground sculpting may be useful when diffuse light is high.

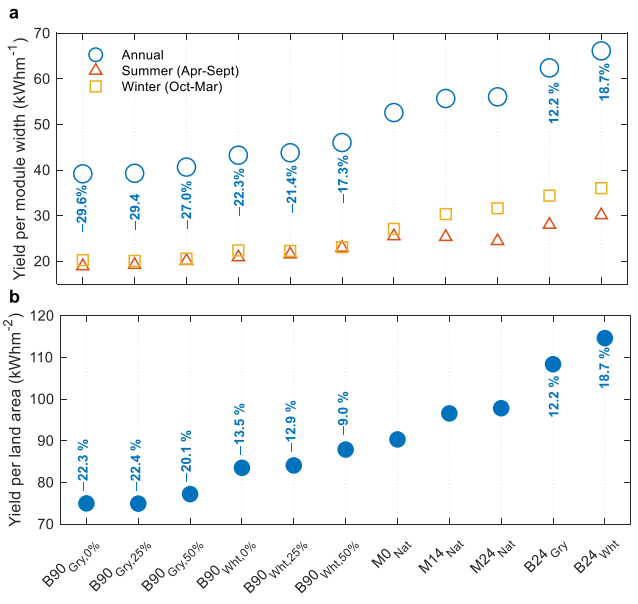

FIGURE 7. **a, Predicted annual yield per row length from each configuration under study. The BG_E for each bifacial configuration is shown. The annual yield is split into yields from half-yearly periods: Summer and Winter. In Winter, with higher availability of direct sunlight compared to in Summer, the TBF configurations produce higher relative yield. b, The predicted annual yield per land area for the experimental configurations. BGE per land area for bifacial configurations are also shown.**

VI. LOCATION-SPECIFIC PERFORMANCE OF OPTIMUM BIFACIAL SOLAR FARMS

We now apply our solar farm model to predict the energy yield performance of TBF and VBF farms for several locations across the globe. Fig. 8(a) shows the annual yield per

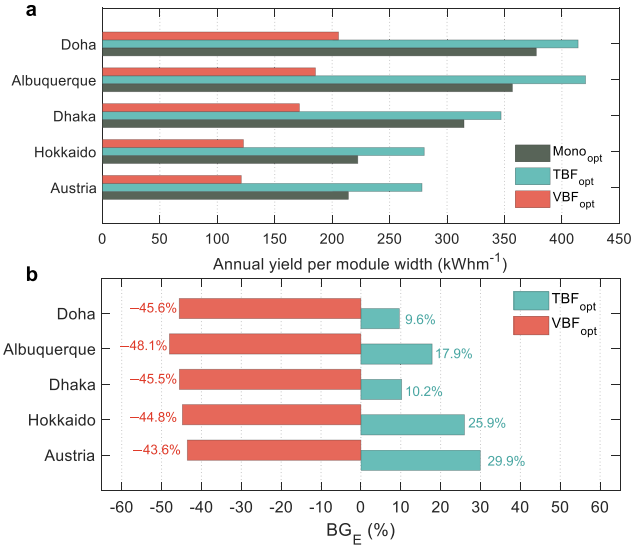

FIGURE 8. **a. Predicted annual yield per module width shown for optimum tilted bifacials (TBF), vertical bifacials (VBF), and monofacials. b. The corresponding BG_E of bifacial solar farms.**

module width (in kW·h·m^{-1}) obtainable from optimum farms TBF$_{opt}$, VBF$_{opt}$ and Mono$_{opt}$ at various geographic locations. To represent the modules in utility-scale solar farms, we set the module M_h to 1 m, and efficiencies η_{dir} and η_{diff} to 18.9% and 15.67%, respectively, and assume $R_A = 0.5$. The farms TBF$_{opt}$ and Mono$_{opt}$ are optimized for minimum LCOE [5]. The modules are assumed to be mounted in an array at a height $y_0 = 1$ m above the ground. One the other hand, the VBF$_{opt}$ farm is optimized for the ground shape r with $p = M_h$ [22]. As observed in Fig. 8(a), Doha has the highest yield — the location-specific variation in output is due to the difference in insolation. As expected, TBF outperforms other configurations.

In Fig. 8(b), we compare the BG$_E$ for the three configurations. At higher latitudes, the modules are optimally tilted at higher angles to follow the sun — this enhances the importance of bifaciality to collect sky-diffuse and albedo light through the back face [5]. That is why we observe higher BG$_E$ at high latitudes such as in Austria ($k_d = 0.53$) and Hokkaido, Japan ($k_d = 0.54$). Doha, Qatar ($k_d = 0.23$) has low annual diffuse fraction, and therefore has the least BG$_E$. Although Dhaka, Bangladesh (23.8°N, $k_d = 0.4$) and Doha (25.3°N) have similar latitudes, we observe a slightly higher BG$_E$ in Dhaka due to higher k_d. The predicted BG$_E$ in Fig. 8(b) are similar to that seen in Table 1 – however, a proper comparison is difficult here as the experiments in literature as listed in the table are not representative of the LCOE-minimized design.

The negative BG$_E$ for VBF configurations in Fig. 8(b) indicates its significantly lower yield compared to Mono$_{opt}$. Indeed, we find that, in terms of yield per module width, the Mono$_{opt}$ outperforms the VBF$_{opt}$ anywhere in the world (see Supplementary Fig. S6). However, when maximum yield per land area is required, the VBF$_{opt}$ are expected to perform better at higher latitudes (see Supplementary Fig. S6). Also, the smaller optimized period ($p = M_h$) [22] compared to our experiments ($p = 1.6\ M_h$) results in lowered albedo light collection and degraded bifacial gain.

VII. EFFECT OF DIFFUSE SUNLIGHT ON OPTIMAL VBF PERFORMANCE

In the experimental data shown in Fig. 4, we observed that ground sculpting by increasing r does not necessarily maximize yield from VBF every day. Remember, we defined 'crossover' as the case when VBF with flat-ground outperformed its ground-sculpted counter-part with the same R_A. The anomalous crossovers in the daily yields largely occurred on clearer days between the B90$_{Wht,\ 0\%}$ and B90$_{Wht,\ 25\%}$ pair, and B90$_{Gry,\ 0\%}$ and B90$_{Gry,\ 50\%}$ pair. The crossovers statistically occur on a minute basis with the variation in the diffuse fraction k_d due to natural changes in the atmospheric conditions. Fig. 9 shows the percentage of crossovers in the measured output (taken every two minutes) of B90$_{Wht,\ 0\%}$-B90$_{Wht,\ 25\%}$ pair at different k_d values. The distribution shows that the crossovers are more likely when k_d is low, i.e., more direct sunlight is available. It suggests that, at locations with low diffuse fraction, the crossovers are more frequent,

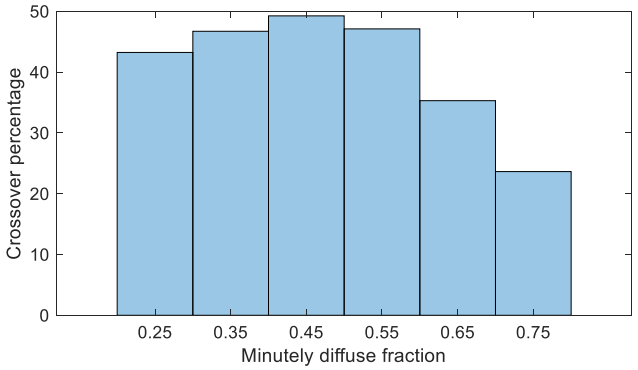

FIGURE 9. Distribution of crossover percentage between B90$_{Wht,\ 25\%}$ and B90$_{Wht,\ 0\%}$ against minutely diffuse fraction. The distribution indicates that the crossovers occurred more frequently when diffuse fraction was low.

and the vertical bifacial configurations with a flat ground may be equivalent or better than ground-sculpted ones.

We, therefore, posit that the conventional flat ground ($r = 0$) VBF may be preferable at locations that experience more direct sunlight (low k_d), while the sculpted ground ($r > 0$) tends to be better at locations with more diffuse sunlight (high k_d). For instance, locations such as Phoenix, USA, have a low annual average diffuse fraction—indicating significant amounts of direct sunlight around the year. Consequently, in such locations, the lack of diffuse sunlight may neutralize the expected benefits of the VBF in the long term. To illustrate this dependency on the local diffuse fraction, we carry out a worldwide simulation of B90$_{Wht,\ 50\%}$ and B90$_{Wht,\ 0\%}$ configurations to estimate the annual gains obtainable with ground-sculpting; the results are shown in Fig. 10. We choose $p = M_h$ for the simulation with module efficiencies η_{dir} and η_{diff} set to 18.9% and 15.67%, respectively [22].

Fig. 10(a) shows the annual diffuse fractions around the world. For such expected irradiance conditions, Fig. 10(b) shows the ratio of the predicted annual yield obtained for B90$_{Wht,\ 50\%}$ and B90$_{Wht,\ 0\%}$ configurations. We find that B90$_{Wht,\ 50\%}$ is expected to yield similar to or higher than B90$_{Wht,\ 0\%}$ all over the globe. However, the relative gains for ground-sculpted B90$_{Wht,\ 50\%}$ diminish at locations with low diffuse fractions (i.e., locations with clearer sky on average), which is consistent with our hypothesis. For instance, in parts of northern Africa and Saudi Arabia, where $k_d < 0.25$, the gains can be only 1–2%. By contrast, for $k_d > 0.4$, the ground-sculpting can lead to ∼30% performance improvement in several parts of the world, e.g., in eastern China. Indeed, we find that the gains for B90$_{Wht,\ 50\%}$ tend to be generally higher for regions with latitudes greater than 30° owing to the higher availability of diffuse sunlight at these regions as shown in Fig. 10(a). The predicted annual BG$_E$ for VBF configurations per row length and per land area shown in Supplementary Fig. S6 – at latitudes > 45° VBF is expected to yield more than monofacials in a finite-sized farm. Our

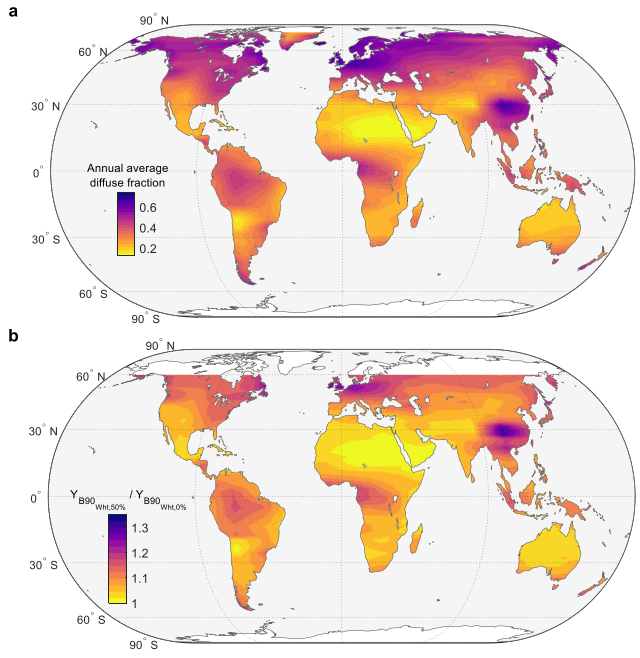

FIGURE 10. **Impact of the availability of diffuse sunlight on the worldwide VBF performance. a, Map showing the annual diffuse fraction calculated based on the data from NASA's POWER database. b, Worldwide predicted annual yield ratio of $B90_{Wht,\ 50\%}$ (optimal VBF) and $B90_{Wht,\ 0\%}$ (conventional flat ground) configurations. The relative gain of ground-sculpted configurations is minuscule at regions near the equator for low values of diffuse fraction. However, the gain increases at higher latitudes with higher diffuse fractions.**

predicted VBF gains are smaller compared to the one reported previously in Ref. [22]. We now predict ground sculpting is expected to improve VBF performance at locations with a higher diffuse fraction.

VIII. CONCLUSIONS

In this work, we have studied ten configurations in outdoor array conditions having varying azimuth, tilt, albedo, and ground height parameters at East West University, Dhaka, Bangladesh. Based on the experimental data, we provide a side-by-side comparison of the yield performance of tilted bifacial (TBF) and vertical bifacial (VBF) arrays. A summary of the work is as follows.

(1) All our configurations are designed to near-optimum spacing from numerical predictions in literature [5]. We observe from our experiments that the best TBF yields 21.3% and 73.3% more compared to the optimal monofacial and VBF, respectively over the two months of experiment in autumn.

(2) Our study includes the effect of ground albedo R_A for multi-row arrays. We observe that by increasing R_A from 0.3 to 0.5: the VBF sees a 16.3% increase, and the TBF has a 2.3% increase in yield. The improvements are relatively moderate compared to that seen in literature. This is due to the smaller period (close to optimum) of the array than that in prior works. We also observe a large statistical variability in TBF yield and bifacial gain on brighter days — this is associated with larger variation in ambient temperature on such days.

(3) The experimental configurations are simulated using Purdue view-factor-based opto-electric solar farm model [5], [22]. The simulated trend shows a remarkably good agreement with the experiments (suggesting the maturity and reliability of these models): the predicted yields for TBF and VBF configurations show 2.7% and 5.5% maximum absolute percentage error, respectively.

(4) Over the experimental study period, the bifacial gain in energy (BG_E) of the best performing VBF and TBF are -30% and 21.3%, respectively. The numerically extrapolated annual BG_E based on *output per farm area* is: -26.8% for VBF and 18.5% for TBF. By including the Perez model to estimate diffuse irradiance, we now predict the gains for ground-sculpted VBF to be significantly smaller than the previous prediction near the tropics [22].

(5) Our experiments demonstrate that the efficacy of the ground-sculpting technique degrades as the location's diffuse sunlight fraction decreases. This characteristic extrapolates to location-specific annual diffuse fraction, as predicted by the numerical model. In a global analysis, we observe that at locations with a clear sky (i.e., low diffuse fraction), the ground-sculpted VBF only provides 3% more yearly yield compared to a VBF farm with a flat, un-patterned ground. In general, VBF outputs less than monofacial farms for all locations within latitude $< 45°$; however, the potential for vertical module arrays would truly be understood once the soiling effects and maintenance costs are factored in for overall LCOE and profit analysis.

The experimental data and the yield predictions reaffirm that fixed tilted bifacial arrays are more efficient than the vertical bifacial ones. However, the inherent geometry of vertical bifacial arrays makes it a natural fit for land-constrained niche applications, such as AgroPV and structure-integrated PV. Furthermore, when we consider soiling losses, the performance of vertical bifacials is expected to improve considerably. A comprehensive techno-economic analysis would be of interest to evaluate such potentials. While this study focuses on maximizing DC generation potential, net economic value of generated renewable power for end user will also depend on tackling challenges related to power quality [47], [48]. Nevertheless, we anticipate the results will help to pave the way for reducing solar LCOE by providing strategies to increase the energy yield through application-specific bifacial PV systems ensuring optimal utilization of local conditions.

APPENDIX
EXPERIMENTAL PROCEDURES
A. SHORT CIRCUIT CURRENT MEASUREMENT AND MAPPING TO MAXIMUM POWER

The module short circuit current was measured by measuring the voltage drop across a 1±5% Ω resistor. The load voltage

was measured using an in-house data acquisition system equipped with a 10-bit successive-approximation analog-to-digital converter. The converter has an absolute accuracy of ±2 Least Significant Bits (LSB): for the chosen 5 V reference voltage the accuracy was ±9.76 mV. Each data point was recorded at 2-minute intervals. Module-to-module output variability is accounted for by multiplying the output by a correction factor (see Supplementary sec. S5).

The module's current-voltage profile and the maximum power output under 1000 $W{\cdot}m^{-2}$ irradiance was obtained by flash testing. As the short circuit current varies with the light collection, the current-voltage profile under varying irradiance can be approximated by shifting the profile vertically. A mapping between the short circuit current and maximum power output was calculated from the shifted profiles (shown in Supplementary Fig. S1). Using the mapping, the daily maximum power profile corresponding to a module's daily short circuit current profile was obtained through linear interpolation and extrapolation.

B. GLOBAL HORIZONTAL IRRADIANCE MEASUREMENT

The global horizontal irradiance (GHI) was estimated from a calibrated horizontal monofacial module. The module was characterized under standard testing conditions (using Optosolar GmbH Flashlight Simulator), where under 1000 $W{\cdot}m^{-2}$ (1 sun) irradiance 2 A short circuit current was measured from the module. This measure was used to calculate the instantaneous GHI in $W{\cdot}m^{-2}$ from the measured module instantaneous short circuit current.

C. DHI AND DIFFUSE FRACTION (k_d) CALCULATION

To calculate the diffuse fraction, in addition to GHI, we need to quantify the diffuse horizontal irradiance. We can calculate the instantaneous diffuse horizontal irradiance from the measured module front and rear face I_{SC} profiles of $B90_{Gry,\ 50\%}$ and $B90_{Wht,\ 50\%}$ configurations. These configurations are identical with the exception of having varying R_A. As discussed before, until noon, the eastward face of the vertical bifacial module receives mostly direct sunlight, but the westward face receives none; and vice versa in the afternoon. By concatenating the morning-time west face and afternoon-time east face profiles, we isolate the diurnal I_{SC} profile owing to diffuse sunlight (see Fig. 3d). The total I_{SC} due to diffuse sunlight, I_{diff}, can be decomposed as

$$\begin{aligned} I_{diff} &= I_{sky} + I_{albedo} \\ &= I_{sky} + R_A I_{ground} \end{aligned} \tag{2}$$

where I_{sky} is the isotropic sky diffuse sunlight component and I_{albedo} is the ground albedo component.

DHI is defined as the diffuse irradiance incident on a horizontal surface from the sky. Therefore, we are only interested in the I_{sky} component, as a horizontally oriented absorber will only receive that component. The $B90_{Gry,\ 50\%}$ and $B90_{Wht,\ 50\%}$ configurations are identical except only the albedo coefficient (R_A) of the ground. With the total I_{diff} and R_A known for the two configurations, we solve the following 2×2 system of equations for I_{sky}.

$$\mathbf{I} = \mathbf{C}^{-1}\mathbf{I_{diff}} \tag{3}$$

where, $\mathbf{C}$ is the coefficient matrix of I_{sky} and I_{ground}, and $\mathbf{I_{diff}}$ is a column vector containing the I_{diff} value of $B90_{Gry,\ 50\%}$ and $B90_{Wht,\ 50\%}$ configurations at a given time. The irradiance value corresponding to the calculated I_{sky} is obtained by applying 500 $W{\cdot}m^{-2}{\cdot}A^{-1}$ conversion factor obtained from module flash testing.

D. ALBEDO COEFFICIENT (R_A) MEASUREMENT

The values of R_A of the vinyl banner covered ground were obtained experimentally. Two back-to-back mounted solar reference cells were placed horizontally at 1 feet above the ground, and their short-circuit currents were measured at solar noon. While light reaches the top cell directly, it has to be reflected from the ground surface before reaching the bottom cell. Therefore, the ratio of the average short-circuit current of the bottom cell to the top cell represents the fraction of light reflected by the ground, namely the albedo coefficient of the ground.

E. NUMERICAL MODEL FOR SOLAR FARM's YIELD PREDICTIONS

Our numerical calculations for the module array yield uses the models from refs. [5], [22]. For the annual yield analysis (both local and global), the 22-year average GHI values are obtained from the NASA POWER database [45]. The clear-sky irradiance [46] is scaled to the GHI data for a more practical estimate. Orgill-Hollands along with Perez correction is used to decompose GHI into DHI and DNI. One difference with Ref. [22] is that we consider the Perez correction for the vertical module arrays.

The contribution of DNI and DHI are treated separately. The direct light collection and relevant shading on the modules and the ground are appropriately modeled by considering the temporal change in the position of the sun. The amount of DHI collection on module faces and the ground are calculated through sky-to-module and sky-to-ground view factors, respectively. The ground is then assumed to be a secondary diffuse light source to find the albedo collection on the module faces. Once the light distribution on the module is known, an electrical model is used to find the output power (later integrated to find energy yield). We consider 3-bypass diodes in the electrical model of the module.

ACKNOWLEDGMENT

The authors would like to thank Loknath Karmakar Himel and Syed Rafayedt Ahmed for their help to do the initial setup. The authors would also like to thank the EWU Engineering Department for their on-site support and Purdue University for providing computational facilities.

REFERENCES

[1] *International Technology Roadmap for Photovoltaic (ITRPV), 2019 Results*, 11 ed., VDMA, Frankfurt, Germany, Oct. 2020.

[2] R. V. K. Chavali, S. De Wolf, and M. A. Alam, "Device physics underlying silicon heterojunction and passivating-contact solar cells: A topical review," *Prog. Photovolt., Res. Appl.*, vol. 26, no. 4, pp. 241–260, Apr. 2018.

[3] *JinkoSolar to Supply Swan Bifacial Modules for Shanghai Electric's DEWA Project Under Strategic Partnership Agreement*, Aug. 2020.

[4] *JinkoSolar to Supply 126 MW of Modules for a Utility PV Project in Chile*, Jul. 2020.

[5] M. T. Patel, M. R. Khan, X. Sun, and M. A. Alam, "A worldwide cost-based design and optimization of tilted bifacial solar farms," *Appl. Energy*, vol. 247, pp. 467–479, Aug. 2019.

[6] E. Molin, B. Stridh, A. Molin, and E. Wackelgard, "Experimental yield study of bifacial PV modules in Nordic conditions," *IEEE J. Photovolt.*, vol. 8, no. 6, pp. 1457–1463, Nov. 2018.

[7] J. Appelbaum, "Bifacial photovoltaic panels field," *Renew. Energy*, vol. 85, pp. 338–343, Jan. 2016.

[8] S. Bhaduri and A. Kottantharayil, "Mitigation of soiling by vertical mounting of bifacial modules," *IEEE J. Photovolt.*, vol. 9, no. 1, pp. 240–244, Jan. 2019.

[9] J. B. Jahangir, M. Al-Mahmud, M. S. S. Shakir, M. M. H. Mithhu, T. A. Rima, R. N. Sajjad, and M. R. Khan, "Prediction of yield, soiling loss, and cleaning cycle: A case study in south Asian highly construction-active urban zone," in *Proc. 47th IEEE Photovoltaic Spec. Conf. (PVSC)*, Jun. 2020, pp. 1371–1374.

[10] C. K. Miskin, Y. Li, A. Perna, R. G. Ellis, E. K. Grubbs, P. Bermel, and R. Agrawal, "Sustainable co-production of food and solar power to relax land-use constraints," *Nature Sustainability*, vol. 2, no. 10, pp. 972–980, Oct. 2019.

[11] M. H. Riaz, R. Younas, H. Imran, M. A. Alam, and N. Z. Butt, "Module technology for agrivoltaics: Vertical bifacial vs. tilted monofacial farms," 2019, *arXiv:1910.01076*.

[12] M. R. Khan, M. T. Patel, R. Asadpour, H. Imran, N. Z. Butt, and M. A. Alam, "A review of next generation bifacial solar farms: Predictive modeling of energy yield, economics, and reliability," *J. Phys. D, Appl. Phys.*, vol. 54, no. 32, May 2021, Art. no. 323001.

[13] A. Cuevas, A. Luque, J. Eguren, and J. del Alamo, "50 per cent more output power from an albedo-collecting flat panel using bifacial solar cells," *Sol. Energy*, vol. 29, no. 5, pp. 419–420, 1982.

[14] Y. Seo, S. Mun, M. Ahn, S. Dittmann, W. K. Kim, H. Park, Y. Yoo, M. Kim, S.-Y. Oh, S. Alhammadi, S. Chang, S.-H. Park, and J. Lee, "Effect of front irradiance and albedo on bifacial gain in 1.8 kW bifacial silicon photovoltaic system," in *Proc. IEEE 46th Photovoltaic Specialists Conf. (PVSC)*, Chicago, IL, USA, Jun. 2019, pp. 1298–1301.

[15] H. Park, S. Chang, S. Park, and W. K. Kim, "Outdoor performance test of bifacial n-type silicon photovoltaic modules," *Sustainability*, vol. 11, no. 22, p. 6234, Nov. 2019.

[16] X. Sun, M. R. Khan, C. Deline, and M. A. Alam, "Optimization and performance of bifacial solar modules: A global perspective," *Appl. Energy*, vol. 212, pp. 1601–1610, Feb. 2018.

[17] J. S. Stein *et al.*, "Bifacial photovoltaic modules and systems: Experience and results from international research and pilot applications," Internation Energy Agency, Paris, France, Tech. Rep., IEAPVPS T13–14:2021, Apr. 2021.

[18] A. A. B. Baloch, S. Hammat, B. Figgis, F. H. Alharbi, and N. Tabet, "In-field characterization of key performance parameters for bifacial photovoltaic installation in a desert climate," *Renew. Energy*, vol. 159, pp. 50–63, Oct. 2020.

[19] D. Berrian, J. Libal, M. Klenk, H. Nussbaumer, and R. Kopecek, "Performance of bifacial PV arrays with fixed tilt and horizontal single-axis tracking: Comparison of simulated and measured data," *IEEE J. Photovolt.*, vol. 9, no. 6, pp. 1583–1589, Nov. 2019.

[20] A. Luque, E. Lorenzo, G. Sala, and S. López-Romero, "Diffusing reflectors for bifacial photovoltaic panels," *Sol. Cells*, vol. 13, no. 3, pp. 277–292, Jan. 1985.

[21] H. Nussbaumer, G. Petrzilek, S. Schartinger, M. Klenk, N. Keller, T. Baumann, F. Carigiet, and F. Baumgartner, "Influence of low concentration on the energy harvest of PV systems using bifacial modules," in *Proc. 32nd Eur. Photovolt. Solar Energy Conf. Exhib.*, Jul. 2016, pp. 2184–2190, doi: 10.4229/EUPVSEC20162016-5BV.4.3.

[22] M. R. Khan, E. Sakr, X. Sun, P. Bermel, and M. A. Alam, "Ground sculpting to enhance energy yield of vertical bifacial solar farms," *Appl. Energy*, vol. 241, pp. 592–598, May 2019.

[23] R. Perez, R. Seals, P. Ineichen, R. Stewart, and D. Menicucci, "A new simplified version of the Perez diffuse irradiance model for tilted surfaces," *Sol. Energy*, vol. 39, no. 3, pp. 221–231, Jan. 1987.

[24] M. T. Patel, R. A. Vijayan, R. Asadpour, M. Varadharajaperumal, M. R. Khan, and M. A. Alam, "Temperature-dependent energy gain of bifacial PV farms: A global perspective," *Appl. Energy*, vol. 276, Oct. 2020, Art. no. 115405.

[25] M. R. Khan, A. Hanna, X. Sun, and M. A. Alam, "Vertical bifacial solar farms: Physics, design, and global optimization," *Appl. Energy*, vol. 206, pp. 240–248, Nov. 2017.

[26] J. S. Stein, D. Riley, M. Lave, C. Hansen, C. Deline, and F. Toor, "Outdoor field performance from bifacial photovoltaic modules and systems," in *Proc. IEEE 44th Photovoltaic Spec. Conf. (PVSC)*, Washington, DC, USA, Jun. 2017, pp. 3184–3189.

[27] I. Shoukry, J. Libal, R. Kopecek, E. Wefringhaus, and J. Werner, "Modelling of bifacial gain for stand-alone and in-field installed bifacial PV modules," *Energy Proc.*, vol. 92, pp. 600–608, Aug. 2016.

[28] T. Katsaounis, K. Kotsovos, I. Gereige, A. Basaheeh, M. Abdullah, A. Khayat, E. Al-Habshi, A. Al-Saggaf, and A. E. Tzavaras, "Performance assessment of bifacial c-Si PV modules through device simulations and outdoor measurements," *Renew. Energy*, vol. 143, pp. 1285–1298, Dec. 2019.

[29] S. A. Pelaez, C. Deline, S. M. MacAlpine, B. Marion, J. S. Stein, and R. K. Kostuk, "Comparison of bifacial solar irradiance model predictions with field validation," *IEEE J. Photovolt.*, vol. 9, no. 1, pp. 82–88, Jan. 2019.

[30] K. Sugibuchi, N. Ishikawa, and S. Obara, "Bifacial-PV power output gain in the field test using 'EarthON' high bifaciality solar cells," in *Proc. 28th Eur. Photovoltaic Sol. Energy Conf. Exhib.*, 2013, pp. 4312–4317.

[31] W. Muehleisen, J. Loeschnig, M. Feichtner, A. R. Burgers, E. E. Bende, S. Zamini, Y. Yerasimou, J. Kosel, C. Hirschl, and G. E. Georghiou, "Energy yield measurement of an elevated PV system on a white flat roof and a performance comparison of monofacial and bifacial modules," *Renew. Energy*, vol. 170, pp. 613–619, Jun. 2021.

[32] H. Nussbaumer, M. Klenk, M. Morf, and N. Keller, "Energy yield prediction of a bifacial PV system with a miniaturized test array," *Sol. Energy*, vol. 179, pp. 316–325, Feb. 2019.

[33] H. Nussbaumer, G. Petrzilek, S. Schartinger, M. Klenk, N. Keller, T. Baumann, F. Carigiet, and F. Baumgartner, "Miniaturized test array as a means to determine the energy harvest of bifacial installations," in *Proc. IEEE 43rd Photovoltaic Spec. Conf. (PVSC)*, Jun. 2016, pp. 2698–2703.

[34] C. W. Hansen, R. Gooding, N. Guay, D. M. Riley, J. Kallickal, D. Ellibee, A. Asgharzadeh, B. Marion, F. Toor, and J. S. Stein, "A detailed model of rear-side irradiance for bifacial PV modules," in *Proc. IEEE 44th Photovoltaic Spec. Conf. (PVSC)*, Jun. 2017, pp. 1543–1548.

[35] U. A. Yusufoglu, T. H. Lee, T. M. Pletzer, A. Halm, L. J. Koduvelikulathu, C. Comparotto, R. Kopecek, and A. Kurz, "Simulation of energy production by bifacial modules with revision of ground reflection," *Energy Proc.*, vol. 55, pp. 389–395, Jan. 2014.

[36] U. A. Yusufoglu, T. M. Pletzer, L. J. Koduvelikulathu, C. Comparotto, R. Kopecek, and H. Kurz, "Analysis of the annual performance of bifacial modules and optimization methods," *IEEE J. Photovolt.*, vol. 5, no. 1, pp. 320–328, Jan. 2015.

[37] S. Guo, T. M. Walsh, and M. Peters, "Vertically mounted bifacial photovoltaic modules: A global analysis," *Energy*, vol. 61, pp. 447–454, Nov. 2013.

[38] G. J. M. Janssen, B. B. Van Aken, A. J. Carr, and A. A. Mewe, "Outdoor performance of bifacial modules by measurements and modelling," *Energy Proc.*, vol. 77, pp. 364–373, Aug. 2015.

[39] A. Asgharzadeh, F. Toor, B. Bourne, M. A. Anoma, A. Hoffman, C. Chaudhari, S. Bapat, R. Perkins, D. Cohen, G. M. Kimball, and D. Riley, "A benchmark and validation of bifacial PV irradiance models," in *Proc. IEEE 46th Photovoltaic Spec. Conf. (PVSC)*, Chicago, IL, USA, Jun. 2019, pp. 3281–3287.

[40] C. W. Hansen, J. S. Stein, C. Deline, S. MacAlpine, B. Marion, A. Asgharzadeh, and F. Toor, "Analysis of irradiance models for bifacial PV modules," in *Proc. IEEE 43rd Photovoltaic Spec. Conf. (PVSC)*, Jun. 2016, pp. 0138–0143.

[41] J. F. Orgill and K. G. T. Hollands, "Correlation equation for hourly diffuse radiation on a horizontal surface," *Sol. Energy*, vol. 19, no. 4, pp. 357–359, Jan. 1977.

[42] P. G. Loutzenhiser, H. Manz, C. Felsmann, P. A. Strachan, T. Frank, and G. M. Maxwell, "Empirical validation of models to compute solar irradiance on inclined surfaces for building energy simulation," *Sol. Energy*, vol. 81, no. 2, pp. 254–267, Feb. 2007.
[43] R. Perez, P. Ineichen, R. Seals, J. Michalsky, and R. Stewart, "Modeling daylight availability and irradiance components from direct and global irradiance," *Sol. Energy*, vol. 44, no. 5, pp. 271–289, 1990.
[44] R. Perez, R. Stewart, R. Seals, and T. Guertin, "The development and verification of the Perez diffuse radiation model," Atmos. Sci. Res. Center, Sandia Nat. Lab., Albuquerque, NM, USA, State Univ. New York, Albany, NY, USA, Tech. Rep. SAND88-7030, 1988.
[45] *NASA Prediction of Worldwide Energy Resources (POWER) Data Access Viewer*, NASA Langley Res. Center, Hampton, VA, USA, 2020.
[46] B. Haurwitz, "Insolation in relation to cloudiness and cloud density," *J. Meteorol.*, vol. 2, no. 3, pp. 154–166, Sep. 1945.
[47] V. Gevorgian and B. O'Neill, "Advanced grid-friendly controls demonstration project for utility-scale PV power plants," Nat. Renew. Energy Lab. (NREL), Golden, CO, USA, Tech. Rep., NREL/TP-5D00-65368, Jan. 2016.
[48] S. Adak, H. Cangi, B. Eid, and A. S. Yilmaz, "Developed analytical expression for current harmonic distortion of the PV system's inverter in relation to the solar irradiance and temperature," *Electr. Eng.*, vol. 103, no. 1, pp. 697–704, Feb. 2021.

JABIR BIN JAHANGIR (Graduate Student Member, IEEE) received the B.Sc. degree in electrical and electronic engineering (EEE) from East West University, Bangladesh, in 2019. Currently, he is a Graduate Research Assistant with the Alam CEED Group, Purdue University, West Lafayette, USA. Previously, he was part of the Khan Sustainable Research Group, East West University, as a Research Assistant. His research interests include computational modeling of photovoltaic systems and solid-state devices.

MD. AL-MAHMUD received the B.Sc. degree from the Department of Electrical and Electronic Engineering, East West University, Dhaka, Bangladesh, in 2019. After his B.Sc. degree, he worked as a Research Assistant (RA) with the East West University Center for Research and Training (EWUCRT), from 2019 to 2020, under the supervision of Dr. M. Ryan Khan. He is currently working as a Data Assistant with the Management Information System Department. His research interests include design of bifacial solar farms and effects of soiling on solar panels.

MD. SHAHADAT SARKER SHAKIR received the B.Sc. degree in electrical and electronic engineering from East West University, Bangladesh. Currently, he is pursuing the M.Sc. degree in information technology with Jahangirnagar University, Bangladesh. He worked as a Research Assistant with the Dr. M. Ryyan Khan's SLR Group, from September 2019 to April 2021. For his undergraduate thesis, he worked on "Implementation and analysis of south facing bifacial solar farms: effects of ground materials and patterns." He is currently working as an Executive Service and Support Engineer.

ANISUL HAQUE (Senior Member, IEEE) has been working as a Professor with the Department of Electrical and Electronic Engineering, East West University, since 2006. He has been a Visiting Faculty with the Tokyo Institute of Technology, Japan; the University of Connecticut, USA; and Clarkson University, USA. His research interests include the physics, modeling, simulation, and characterization of nanoelectronic devices and photovoltaic devices and systems. He is also interested in engineering education.

He serves on the Board of Accreditation for Engineering and Technical Education (BAETE) and the Institute of Engineers, Bangladesh (IEB), as a Board Member. He has been serving as an IEEE Distinguished Lecturer, since 2009. He was the recipient of the Bangladesh University Grants Commission Award, in 2006; and the Gold Medal from the Bangladesh Academy of Science, in 2010. He has conducted many training and workshop sessions on outcomes based education (OBE) for academic program leaders and on outcomes based accreditation (OBA) for BAETE program evaluators. He was an Editor of IEEE TRANSACTIONS ON ELECTRON DEVICES, from 2010 to 2019. Currently, he is serving as an Associate Editor for IEEE ACCESS.

MUHAMMAD A. ALAM (Fellow, IEEE) is the Jai N. Gupta Professor of electrical engineering with Purdue University, where his research interests include physics, simulation, characterization, and technology of classical and emerging electronic devices, including reliability of scaled MOSFET, theoretical foundation of nano-bio sensors, and atom-to-farm performance and modeling of solar cells. His work has been recognized by the 2006 IEEE Kiyo Tomiyasu Medal, the 2015 SRC Technical Excellence Award, and the 2018 IEEE EDS Education Award.

M. RYYAN KHAN (Member, IEEE) received the B.Sc. degree in electrical and electronic engineering from BUET, Bangladesh, in 2009, and the Ph.D. degree from Purdue University, West Lafayette, USA, in 2016. He was with the Alam CEED Group, Department of Electronics and Communication Engineering, Purdue University, as a Postdoctoral Research Associate, until October 2017. He is currently an Associate Professor with East West University, Dhaka, Bangladesh. His research interests include optical designing and modeling of solar cells, design of bifacial solar farms, effects of soiling on solar panels, and techno-economics of agrivoltaics.